Supporting Information

Interfacial Microdroplets Reshape the Oxidation Pathways of Polycyclic Aromatic Hydrocarbons

Ming Li[a,c], Yueyue Chen[b,c], Menghan Jiang[a,c], Chen Yang[b,c], Ying Xi[a,c], Di Huang[b,c*], Shichao Zhang[a,c], Yingping Huang[a,c], Chuncheng Chen[c,d*]

[a] College of Hydraulic and Environmental Engineering, China Three Gorges University, Yichang 443002, P.R. China;

[b] College of Materials and Chemical Engineering, China Three Gorges University, Yichang 443002, Hubei, P.R. China;

[c] Engineering Research Center of Eco-environment in Three Gorges Reservoir Region, Ministry of Education, China Three Gorges University, Yichang, 443002, P.R. China;

[d] Beijing National Laboratory for Molecular Sciences, Key Laboratory of Photochemistry, CAS Research/Education Center for Excellence in Molecular Sciences, Institute of Chemistry, Chinese Academy of Sciences, Beijing 100190, P.R. China.

Corresponding Authors:

Prof. Di Huang Email: huangdi@ctgu.edu.cn

Prof. Chuncheng Chen Email: ccchen@iccas.ac.cn

Numbers of pages: 16

Numbers of Figures: 9

Numbers of Tables: 3

Text S1 Chemicals and Materials

NAP, PHE, PYR, and FLU, n-Hexane were all purchased from Shanghai Aladdin Biochemical Technology Co., Ltd. Methanol, Isopropanol, Isobutanol, n-Octanol, Acetonitrile, Sodium Dodecyl Sulfate (SDS), Hexadecyl Trimethyl Ammonium Chloride (CTAC), 1,4-Benzoquinone (PBQ), Tert-Butanol (TBA), L-Histidine, Terephthalic Acid (TA), 2-Hydroxyterephthalic Acid were all purchased from Shanghai Macklin Biochemical Co., Ltd. 2,2,6,6-Tetramethylpiperidone (TEMP), and 5,5-Dimethyl-1-Pyrroline N-Oxide (DMPO) were all purchased from Beijing InnoChem Science & Technology Co., Ltd. All chemicals were at least analytical grade and were used without further purification. All solutions were prepared using ultrapure water (18.2 MΩ cm) obtained from the Milli-Q ultrapure water system.

Text S2 Quantitative Analysis of PAHs

PAH concentrations were determined by high-performance liquid chromatography (HPLC, Waters e-2695) equipped with a photodiode array (PDA) detector at $\lambda = 254$ nm. Separation was achieved using a C18 reversed-phase PAH column (4.6 × 250 mm, 5 μm) with isocratic elution (acetonitrile/water = 70:30 v/v) at 30°C.

Text S3 ROS detection, quantification, and quenching experiments

Reactive oxygen species (ROS) generated in the microdroplet system were detected using electron paramagnetic resonance spectroscopy (Magnettech ESR5000, BRUKER). The EPR parameters were as follows: magnetic field strength, 3500.00 G; scan width, 200.00 G; scan time, 30.00 s; microwave power, 19.45 mW; modulation amplitude, 1.000 G; conversion time, 40.0 ms; and microwave frequency, 9.85 GHz. During nebulization, DMPO was used as the spin-trapping agent to detect hydroxyl radical (·OH) and superoxide radical ($O_2^{\cdot-}$), while TEMP was used as the probe to detect singlet oxygen ($^1O_2$).

Hydroxyl radical was quantified using TA as a chemical probe[4]. TA was added to the reaction solution at a final concentration of 5 mM before nebulization. In the presence of ·OH, TA reacts with ·OH to form 2-hydroxyterephthalic acid, which was quantified as an indirect indicator of ·OH formation.

To assess the contribution of different ROS species to PAH degradation, quenching experiments were conducted by adding representative scavengers to the reaction solution before nebulization. TBA, PBQ, and L-histidine were used as scavengers for ·OH, $O_2^{\cdot-}$, and $^1O_2$, respectively. The final concentration of each scavenger was fixed at 10 mM. The scavenger-containing solutions were subjected to the same nebulization conditions as the scavenger-free control. The degradation efficiencies of PAHs in the presence of different scavengers were then compared with those in the control system to evaluate the relative contribution of ·OH, $O_2^{\cdot-}$, and $^1O_2$ to PAH transformation. All experiments were performed in triplicate, and the results are presented as mean ± standard deviation.

Text S4 GC-MS analysis

After ultrasonic atomization reaction, 20 mL of the reaction solution was extracted three times with 10 mL of n-hexane each time. The combined extracts were concentrated to 1 mL under a gentle nitrogen stream prior to GC-MS analysis. Helium was used as the carrier gas at a constant flow rate of 1.0 mL/min. Samples were injected in splitless mode at 300 °C. The oven temperature program was as follows: hold at 60 °C for 1 min, ramp at 5 °C/min to 300 °C, and hold at 300 °C for 5 min. The ion source temperature was maintained at 230 °C, and mass spectra were recorded over the m/z range of 50-500.

Text S5 ESI-MS analysis

Reaction solutions were directly injected and analyzed over an m/z range of 50-300. The operating parameters were as follows: capillary voltage 4.5 kV, sampling cone voltage 50 V, cone voltage 30 V, and dwell time 0.3 s. The desolvation gas temperature was set to 700 ℃, with desolvation and nebulizing gas flow rates of 8.0 L/min and 1.2 L/min, respectively.

Text S6 Classical MD Simulations

The simulations were conducted in a composite system comprising the gas phase, the air-water interface, and the bulk water layer. PAH molecules were initially placed in the gas phase, with their structures described using the General Amber Force Field (GAFF). Water molecules were modeled using the TIP3P water model. All

simulations were performed under the NVT ensemble at 293.15 K, consistent with experimental conditions. The PMF profiles were obtained using umbrella sampling to evaluate the free energy change associated with the translocation of PAHs across the interface.

Text S7 Quantum Chemical Calculations

To investigate the reactive sites of PHE, the frontier molecular orbital characteristics were analyzed. The nucleophilicity index was evaluated based on the HOMO energy, calculated at the B3LYP/6-31G* level[1]. For mechanistic elucidation of the degradation pathways, geometry optimizations of all key intermediates and transition states were performed at the B3LYP-D3(BJ)/6-31+G* level. Subsequently, single-point electronic energies were refined using the B3LYP-D3(BJ)/ma-def2-TZVP basis set to ensure greater accuracy in the relative energy comparisons[2].

Text S8 Photolytic Degradation

Fenton oxidation experiments were performed by adding freshly prepared Fe(II) (6.67 μM) and hydrogen peroxide (20 μM) to the PHE solution (2 μM). The initial pH was adjusted to 3.0 using dilute sulfuric acid to maintain optimal reaction conditions. The reaction mixture was magnetically stirred throughout the experiment.

Photolysis experiments were carried out using a xenon lamp equipped with a band-pass filter (300-400 nm) as the light source. For each experiment, 30 mL of the PHE solution (2 μM) was transferred into a quartz reactor and magnetically stirred during irradiation.

Photolytic Hydrogen Peroxide experiments were carried out under the same irradiation conditions described for photolysis. Hydrogen peroxide was introduced at an initial concentration of 100 μM.

Table S1. The basic physical and chemical properties of polycyclic aromatic hydrocarbons

PAHs	Molecular Formula	Structure	$LogK_{ow}$
Naphthalene	$C_{10}H_8$		3.3
phenanthrene	$C_{14}H_{10}$	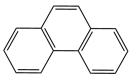	4.46
Pyrene	$C_{16}H_{10}$	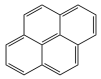	4.88
Fluoranthene	$C_{16}H_{10}$	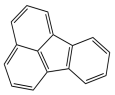	5.16
Glyphosate	$C_3H_8NO_5P$	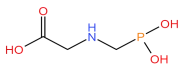	-3.5
ciprofloxacin	$C_{17}H_{18}FN_3O_3$	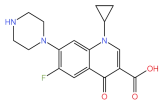	0.28

Table S2. The basic physical and chemical properties of the alcohols

Alcohols	Molecular Formula	Structure	Log P	Solubility
Methanol	CH_4O		-0.77	Miscible with water
Isopropanol	C_3H_8O		0.05	1.66 mol/L
Isobutanol	$C_4H_{10}O$	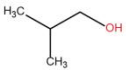	0.76	0.90-1.23 mol/L
n-Octanol	$C_8H_{18}O$		3.00	0.004 mol/L

Table S3. The Fukui index and NPA charge distribution of PHE

Atom	No	Charge (0) e/Å	Charge (+1) e/Å	Charge (-1) e/Å	f^-	f^+	f^0
C	1	-0.0415	-0.0817	-0.0026	0.0390	0.0401	0.0395
C	2	-0.0408	-0.1135	0.0332	0.0740	0.0727	0.0734
C	3	-0.0397	-0.0807	0.0048	0.0445	0.0411	0.0428
C	4	0.0008	-0.0223	0.0229	0.0222	0.0230	0.0226
C	5	-0.0023	-0.0277	0.0223	0.0246	0.0254	0.0250
C	6	-0.0396	-0.0908	0.0191	0.0587	0.0512	0.0550
C	7	0.0008	-0.0223	0.0229	0.0222	0.0230	0.0226
C	8	-0.0023	-0.0277	0.0223	0.0246	0.0254	0.0250
C	9	-0.0414	-0.1245	0.0409	0.0823	0.0831	0.0827
C	10	-0.0414	-0.1245	0.0409	0.0823	0.0831	0.0827
C	11	-0.0397	-0.0807	0.0048	0.0445	0.0411	0.0428
C	12	-0.0408	-0.1135	0.0332	0.0740	0.0727	0.0734
C	13	-0.0415	-0.0817	-0.0026	0.0390	0.0401	0.0395
C	14	-0.0396	-0.0908	0.0191	0.0587	0.0512	0.0550
H	15	0.042	0.0115	0.0719	0.0298	0.0305	0.0302
H	16	0.0413	0.0022	0.0768	0.0355	0.0391	0.0373
H	17	0.0392	0.0163	0.0626	0.0233	0.0230	0.0232
H	18	0.0403	0.0103	0.0699	0.0296	0.0300	0.0298
H	19	0.0414	0.0007	0.0779	0.0365	0.0408	0.0386
H	20	0.0414	0.0007	0.0779	0.0365	0.0408	0.0386
H	21	0.0392	0.0163	0.0626	0.0233	0.0230	0.0232
H	22	0.0413	0.0022	0.0768	0.0355	0.0391	0.0373
H	23	0.042	0.0115	0.0719	0.0298	0.0305	0.0302
H	24	0.0403	0.0103	0.0699	0.0296	0.0300	0.0298

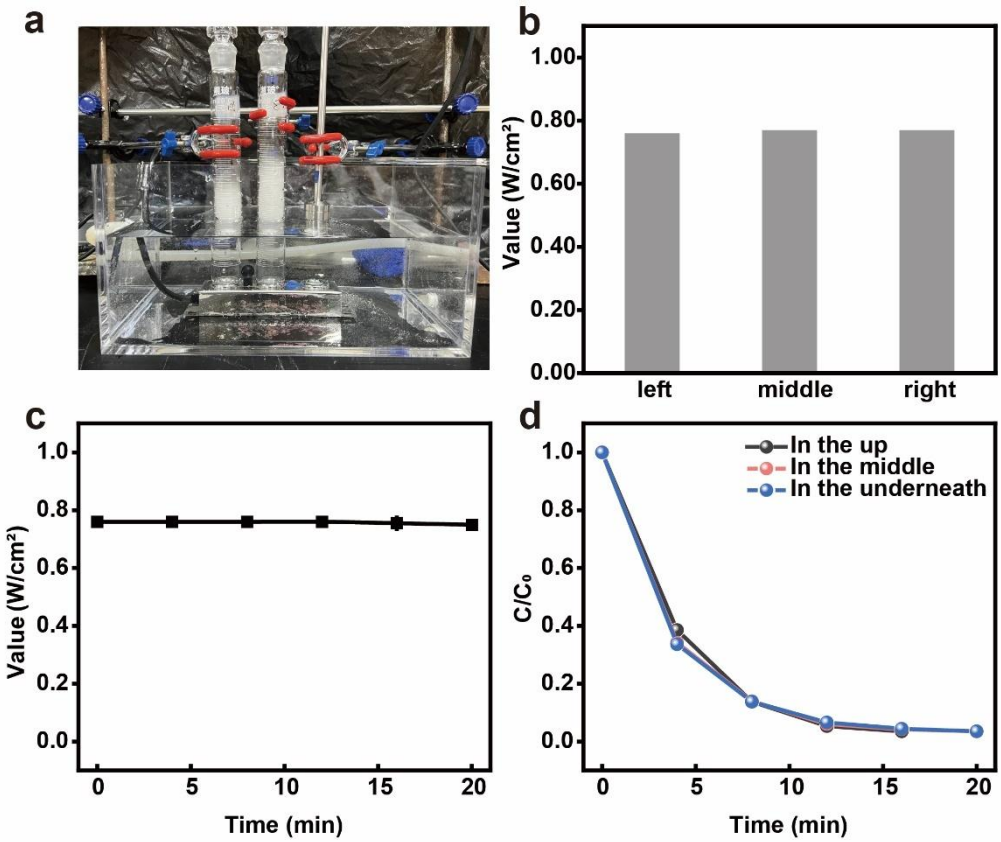

Figure S1. The stability of the microdroplet systems. (a) the ultrasonic intensity at the left, middle, and right positions; (b) The intensity of the ultrasonic during the reaction process; (c)The degradation kinetics of phenanthrene at three different heights; (d) The degradation kinetic curves of PHE in the up (black line), middle (red line) and underneath (blue line) positions of ultrasonic atomization units.

This system generates microdroplet through ultrasonic excitation, significantly increasing the air-water interfacial area and thereby facilitating interfacial reactions. It consists of three independent ultrasonic atomization units with uniformly distributed ultrasonic intensities across the channels, and no significant deviations were observed (Figure S1b). Moreover, the system exhibits excellent temporal and spatial stability (Figure S1c, d), providing a reliable experimental foundation for pollution degradation in microdroplet-based reaction systems.

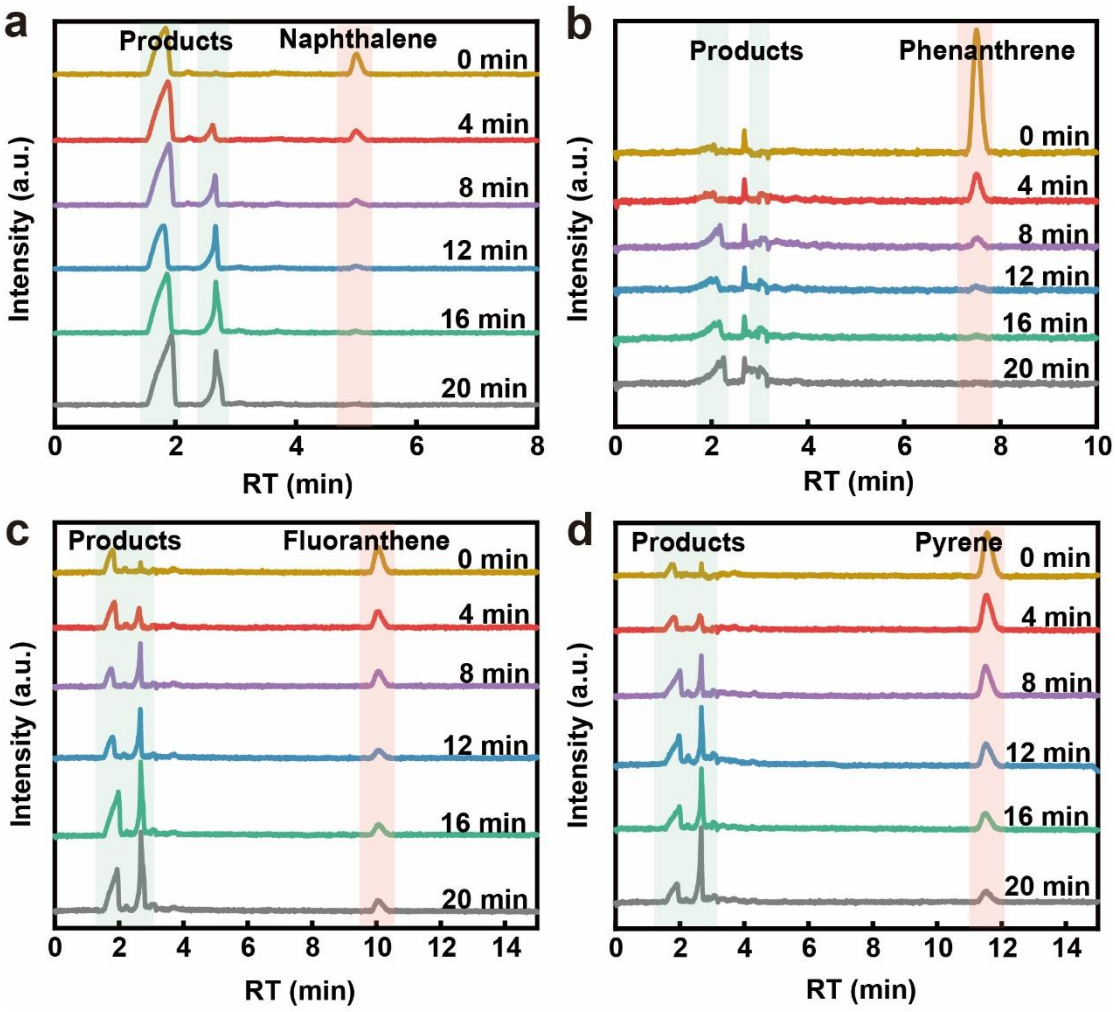

Figure S2. The liquid chromatograms of PAHs in microdroplet systems. (a) Naphthalene; (b) Phenanthrene; (c) Fluoranthene; (d) Pyrene.

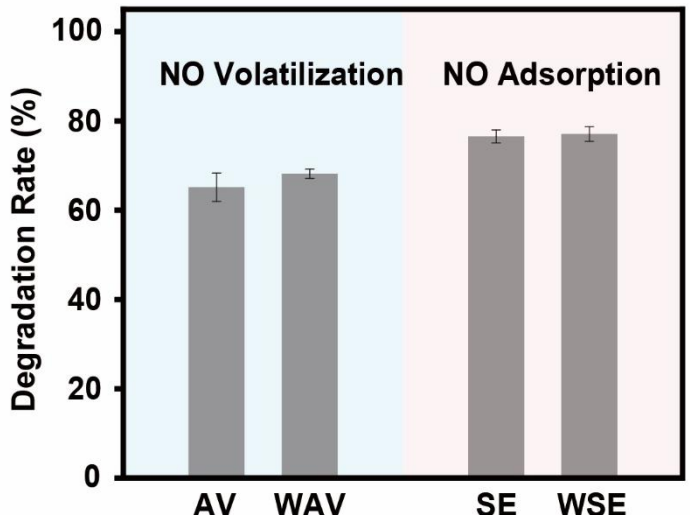

Figure S3. Verification of PHE degradation stability under different treatments. Air ventilation (AV, 100 ml/min, 80%N_2 and 20%O_2) compared with without air ventilation (WAV) and solvent extraction (SE) compared with without solvent extraction (WSE) ($[PHE]_0$= 2 μM).

The Figure S3a shows that the relative concentrations of PAHs remain nearly unchanged after air bubbling (AV) and solvent extraction using acetonitrile (SE), compared with control sample (WAV, WSE). The results indicates that volatilization and adsorption are negligible during the ultrasonic atomization degradation experiments. This confirms that the observed degradation is not caused by physical loss but by reaction transformation in microdroplet systems.

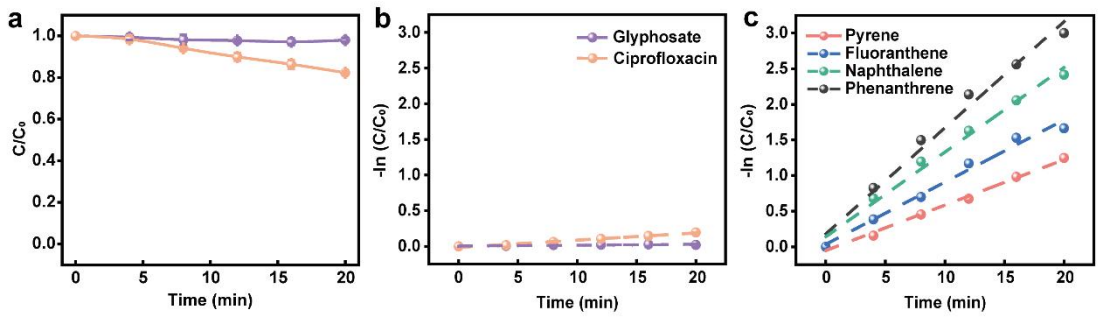

Figure S4. Degradation of organic pollutants in microdroplet systems. (a) The degradation kinetic curves of glyphosate and ciprofloxacin in microdroplet systems; (b) The degradation rate fitting curves of glyphosate and ciprofloxacin in microdroplet systems; (c) The degradation rate fitting curves of PAHs in microdroplet systems.

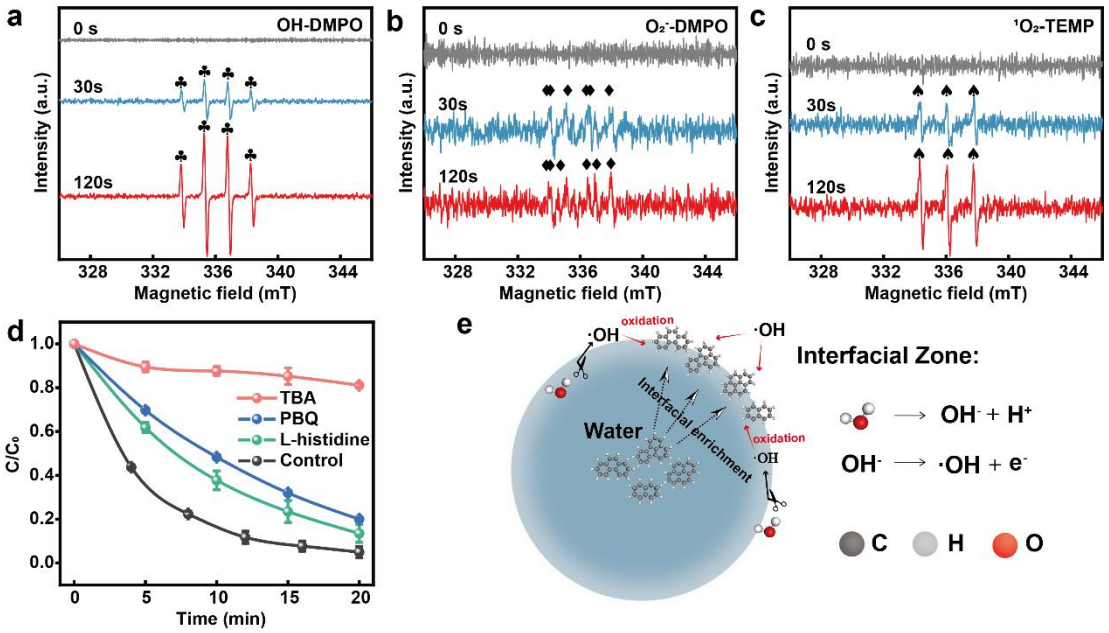

Figure S5. Detection and role of ROS at microdroplet surfaces. (a, b) Trapping signals of ·OH and $O_2^{\cdot-}$ with DMPO detected by EPR spectroscopy; (c) Trapping signals of $^1O_2$ with TEMP detected by EPR spectroscopy; (d) radical quenching experiments for PHE degradation in the presence of different scavengers; (e) schematic illustration of the enrichment effect and ROS generation pathways at microdroplets surface.

To determine the dominant reactive species responsible for PAHs degradation in microdroplet system, EPR spectroscopy with spin-trapping agents was used for in situ detection of reactive ROS.

As shown in Figure S5a, an EPR signal with a characteristic 1:2:2:1 intensity ratio was clearly detected during the atomization microdroplets system, and its intensity increased markedly over time, indicating the continuous and efficient generation of·OH. In addition, the EPR spectra also showed the formation of the superoxide anions $O_2^{\cdot-}$ (Figure S5b) and $^1O_2$ (Figure S5c) over time.

To further quantify the contributions of different ROS to the degradation process, radical scavenging experiments were performed (Figure S5d). The results showed that the addition of the ·OH scavenger tert-butanol (100 mM) almost completely suppressed PHE degradation, confirming ·OH as the predominant reactive species. In contrast, the $O_2^{\cdot-}$ and $^1O_2$ caused moderate reductions in degradation rates, indicating a limited contribution from $O_2^{\cdot-}$ and $^1O_2$ under the current experimental conditions.

At the air-water interface, strong electric fields promote the generation of ROS, creating a highly oxidative microenvironment[3]. The interfacial enrichment of PAHs increases their local concentration near the spontaneously generated ROS, thereby enhancing the degradation of PAHs. Therefore, the rapid PAHs degradation in microdroplet systems arises from a synergistic mechanism (Figure S5e): (i) pronounced interfacial enrichment of hydrophobic PAHs increases their local concentration at the reactive sites, (ii) atomization generates relatively high concentration of interfacial ROS, especially ·OH, and (iii) the confinement of both ·OH and PAHs within a thin interfacial layer maximizes their collision frequency, driving efficient oxidative transformation.

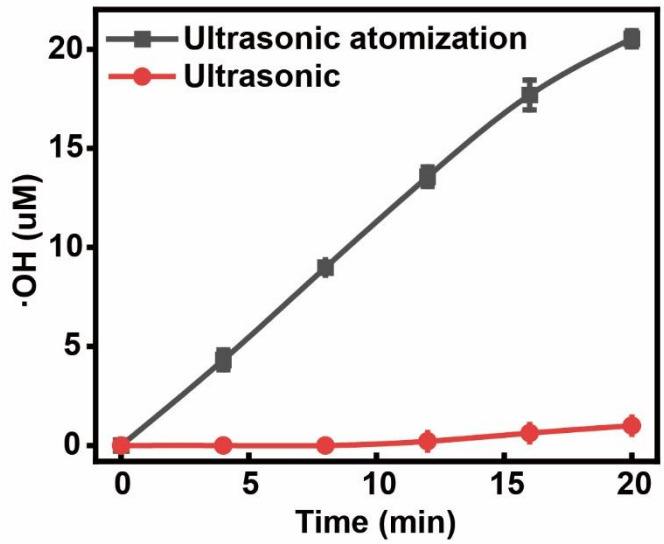

Figure S6. Variation of ·OH concentration over time in microdroplet systems.

The ·OH concentration increased rapidly during the 20 minutes of atomization, (reaching approximately 20.53 μM at 20 minutes), which aligns closely with the independent measurement of 25.58 μM by Shengmao Chao et al.[4], together confirming the production of ·OH at microdroplet surfaces.. However, the ·OH concentration remained at an extremely low level during the 20 minutes of ultrasonic without atomization. The results indicate that ·OH can be sustained and efficient generated throughout the atomization process by microdroplets.

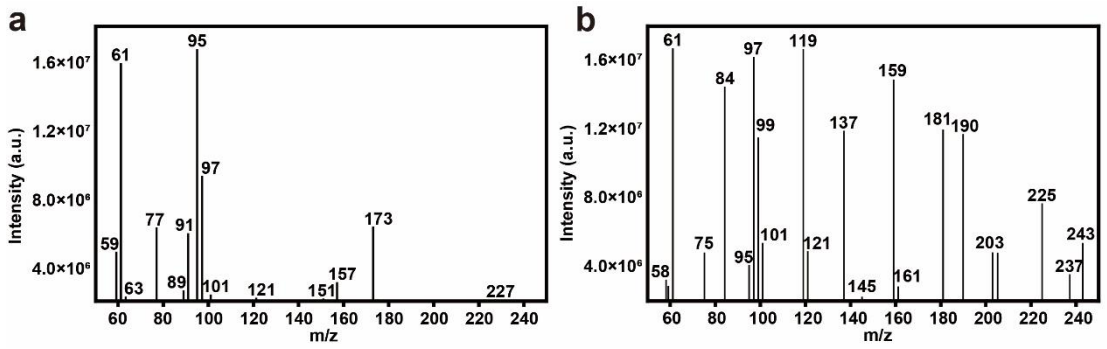

Figure S7. Mass spectra obtained under negative ion modes in in Advanced Oxidation Systems and Microdroplet Systems. (a) Mass spectra obtained under negative ion modes of initial solution before the reaction in Photolysis systems and microdroplet systems; (b) Mass spectra obtained under negative ion modes of initial solution before the reaction in Fenton systems and Photolytic Hydrogen Peroxide systems.

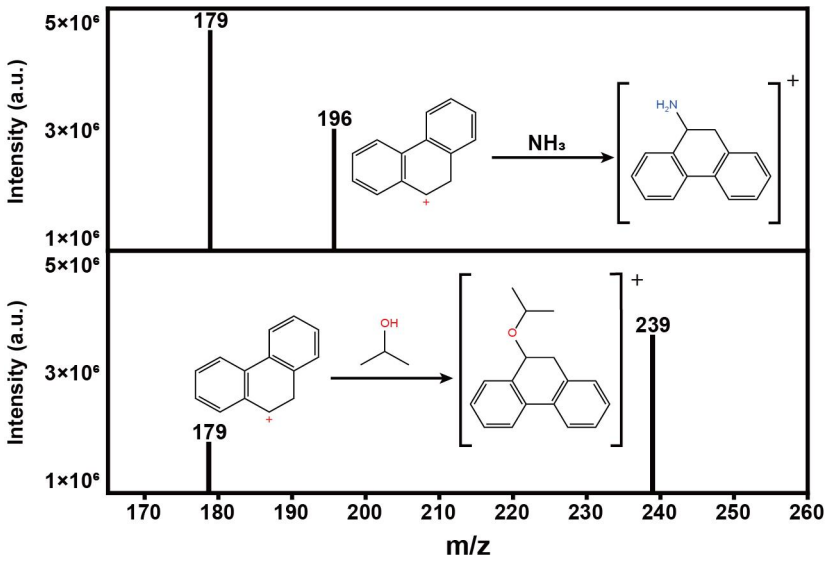

Figure S8. Carbocation-trapping experiments. The initial concentration of phenanthrene was 10 μM, the concentration of ammonia solution and isopropanol were 2 mM.

To probe the possible carbocation intermediate, ammonia solution and isopropanol were selected as nucleophilic trapping agents1. As shown in Figure S8 after the addition of these trapping reagents, new MS signals corresponding to the respective trapping products were observed, supporting the involvement of a cationic intermediate during the interfacial transformation process.

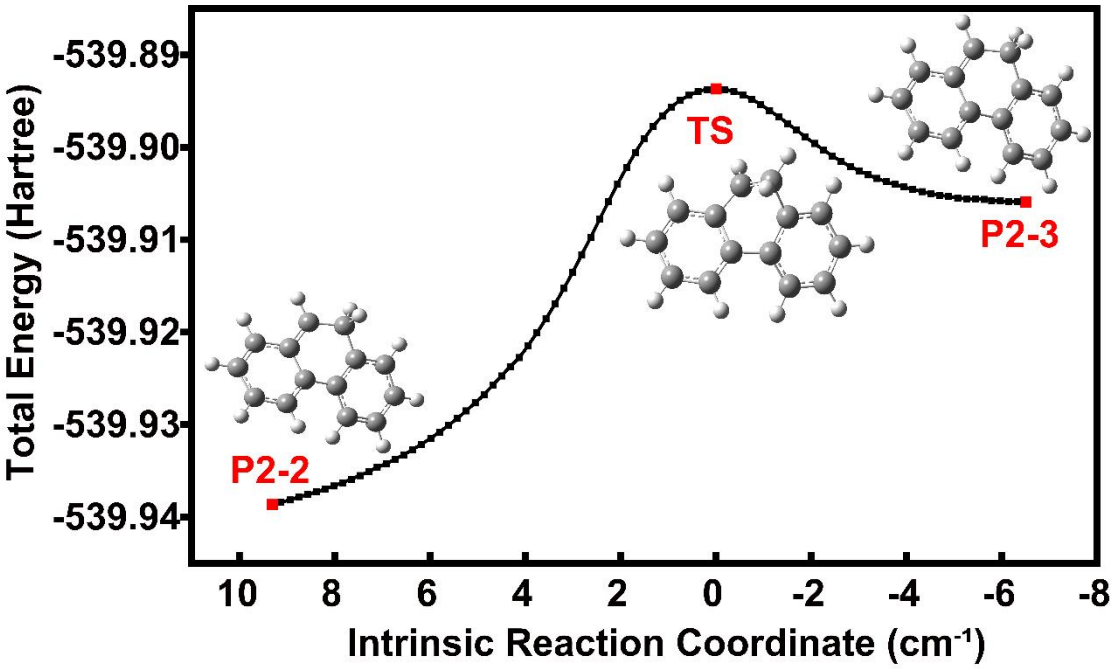

Figure S9. Transition-state and IRC analysis for the P2-2 to P2-3 rearrangement step

In the carbocation-mediated rearrangement pathway, an activation barrier was observed for the P2-2 to P2-3 step. Therefore, we performed transition-state analysis and intrinsic reaction coordinate (IRC) calculations for this step. As shown in Figure S8, the transition state is located at the maximum of the IRC energy profile, and the IRC calculation connects the reactant-like P2-2 structure and the product-like P2-3 structure. This result verifies that a transition state exists for the P2-2 to P2-3 rearrangement step and supports the kinetic feasibility of the proposed 1,2-aryl migration pathway.

References

1. Li, T.; Wang, M.; Hou, Q.; Hou, Y.; Xuan, K.; Hao, Y., Visible-light-enhanced-hydrophilicity promoted adsorption-photodegradation of phenanthrene with core-shell Fe3O4@SiO2@N-TiO2 loaded on graphene oxide. *Appl. Surf. Sci.* **2022,** *605*, 154672.

2. Chen, S.; Li, X.; Fang, Y.-G.; Liu, X.; Yao, Y.; Chen, B.; Francisco, J. S.; Zhu, C.; Chu, C., Accelerated Fatty Acid Oxidation Occurs at the Water-Air Interface of Sea Spray Microdroplets. *J. Am. Chem. Soc.* **2025,** *147*, (42), 38609-38614.

3. Li, F.; Lv, J.; He, A.; Xu, J.; Zhao, L.; Wang, X.; Mao, L.; Li, S.; Wang, H.; Wang, Y.; Jiang, G., Unexpected Generation of Singlet Oxygen at the Air-Water Interface of Aqueous Microdroplets. *J. Am. Chem. Soc.* **2025,** *147*, (34), 30574-30581.

4. Chao, S.; Valsecchi, C.; Sun, J.; Shao, H.; Li, X.; Tang, C.; Fan, M., Highly Sensitive Surface-Enhanced Raman Scattering Detection of Hydroxyl Radicals in Water Microdroplets Using Phthalhydrazide/Ag Nanoparticles Nanosensor. *Environ. Sci. Technol.* **2024,** *58*, (37), 16497-16506.